Available online at www.sciencedirect.com
ScienceDirect
Ceramics International 37 (2011) 1935–1945
CERAMICS INTERNATIONAL
www.elsevier.com/locate/ceramint

Basic slag attack of spinel-containing refractory castables

M.A.L. Braulio [a,*], A.G. Tomba Martinez [b], A.P. Luz [a], C. Liebske [c], V.C. Pandolfelli [a]

[a] *Federal University of São Carlos, Materials Engineering Department, Materials' Microstructural Engineering Group (GEMM – FIRE Associate Laboratory), Rod. Washington Luis, km. 235, 13565-905, São Carlos, Brazil*
[b] *Materials Science and Technology Research Institute (INTEMA), Ceramics Division, Argentina*
[c] *Tata Steel RD&T, Ceramics Research Centre, The Netherlands*

Received 13 January 2011; received in revised form 12 February 2011; accepted 15 February 2011
Available online 23 February 2011

Abstract

The better performance of spinel-containing refractory castables when in contact with basic slag is mainly associated with their higher corrosion resistance. Although the literature has shown various studies related to this subject, only few of them evaluated the overall microstructural effect on the corrosion resistance. Considering this aspect, four different compositions were produced, in order to evaluate the binder source influence (calcium aluminate cement or hydratable alumina), the silica fume addition and spinel incorporation method (*in situ* or pre-formed) effects. Based on the physical properties (apparent porosity, linear thermal expansion and pore size diameter distribution) and also on the phases generated (detected by SEM, before and after corrosion), a basic slag corrosion mechanism, for the set conditions, is proposed. The results pointed out that lower penetration can be attained by reducing the pore size diameters, whereas chemical corrosion resistance is a consequence of higher content of fine alumina, lower amount of calcium aluminates and the lack of liquid phase in the castable matrix. This study stresses that the castable formulation design and the proper raw material selection are of utmost importance to understand and master the performance of this class of refractory castables.

Keywords: E. Refractories; D. Spinels; C. Corrosion

1. Introduction

Pre-formed and *in situ* spinel ($MgAl_2O_4$) containing refractory castables have being widely used as steel ladle linings, due to their high corrosion resistance to basic slag. Various authors [1–4] investigated the slag resistance and wear mechanisms of spinel castables, pointing out that optimal spinel content would be in the 20–25 wt% range. Whereas too little spinel content leads to a high corrosion rate, a too high one results in high penetration [5]. Besides the total amount of spinel, its particle size also affects the corrosion resistance and the finer the spinel grains, the higher the corrosion resistance [5]. In this context, the *in situ* spinel formation in the castable's matrix, by adding magnesia to the high-alumina composition, could result in finer spinel and a better distribution throughout the refractory microstructure, increasing slag penetration and corrosion resistance [6,7].

Other castable raw materials, such as the binder source and fumed silica, can also affect the slag penetration and corrosion resistance. Yamamura et al. [8] investigated the effect of calcium aluminate cement (CAC) content in spinel-containing castables and detected increasing corrosion for the higher cement content compositions, but decreasing penetration. According to Parr et al. [9], the formation of calcium aluminate phases (CA, CA_2 and CA_6) results in a highly densified layer with low open porosity (<10%) and, associated with the spinel presence and alumina, CAC-bonded spinel castables can attain an optimized basic slag resistance. Nevertheless, the formation of CA_2 and CA_6 must be mastered, as it is followed by volumetric expansion and, thus can result in crack generation [10].

Furthermore, Zhou et al. [11] compared the properties of Al_2O_3–MgO refractory castables containing CAC or hydratable alumina as the dominant binder, pointing out better slag infiltration resistance and lower erosion for the cement-free composition. Additions of even small amounts of silica fume to

* Corresponding author.
E-mail address: mariana.gemm@gmail.com (M.A.L. Braulio).

0272-8842/$36.00
doi:10.1016/j.ceramint.2011.02.007

alumina-spinel castables are also detrimental for slag and corrosion resistance [12]. For the same silica fume content, Yilmaz [13] observed better slag infiltration and corrosion resistance for spinel-forming castables than the ones for spinel-containing castables. However, according to Schnabel et al. [14] preformed or *in situ* spinel containing castables present different formulation concepts: whereas alumina–magnesia compositions require silica fume in their composition, mainly in order to counterbalance the *in situ* spinel expansion effects [15,16], preformed spinel castables can be produced without adding silica fume.

Sarpoolaky et al. [17] evaluated the influence of the aggregates source (white-fused alumina, tabular alumina, brown-fused alumina and alumina-rich spinel) on slag corrosion of low-cement containing castables. According to these authors, the chemical attack of the bond system took place firstly in the CaO–MnO–FeO-rich liquid slag and the matrix components (calcium aluminates and alumina). Thus, the local liquid (predominantly $CaO–Al_2O_3–SiO_2$) presented a higher amount of CaO that could react with the grain (generally leading to CA_6 formation). After the dissolution of the finest particles of the matrix, the resultant liquid would then be prone to attack the grains.

Zhang et al. [18] compared the corrosion of alumina grains (white-fused and tabular) by FeO and MnO containing $CaO–MgO–Al_2O_3–SiO_2$ slag and detected the formation of CA_6 and hercynitic spinel ($FeO{\cdot}Al_2O_3$) layers at the alumina-slag interfaces. For tabular alumina, these layers were incomplete, resulting in a direct attack of the slag via pores and grain boundaries. In addition, Vázquez et al. [19] evaluated the corrosion of polycrystalline corundum and calcium hexaluminate by calcium silicate slag, pointing out a homogeneous reaction front for alumina, whereas hibonite (CA_6) led to an irregular reaction front. This aspect was attributed to the open microstructure generated by the CA_6 formation, which could be easily penetrated by slag, through the porosity and the grain boundaries.

Although the literature has widely studied the slag corrosion behavior of Al_2O_3–MgO containing refractories, very few studies have evaluated the overall castable microstructure effect on the corrosion resistance and stated a general corrosion mechanism for this sort of castables. Therefore, this work addresses the analysis of four different spinel-containing refractory castables in order to compare the effect of silica fume and the binder source (in alumina–magnesia refractory castables) and also the spinel incorporation method (*in situ* versus preformed for CAC and silica fume-containing compositions). Based on the castable microstructures and its effect on the slag attack behavior, a corrosion mechanism, for the testing conditions, is proposed, pointing out the importance of a suitable castable composition design in order to extend the working life of the refractory.

2. Materials and techniques

Different vibratable castable compositions were designed using Alfred's particle packing model ($q = 0.26$) [20]. Three of them were *in situ* spinel-forming castables (Al_2O_3–MgO based) and the other a pre-formed spinel-containing one. For the spinel-forming compositions, their matrix comprised 6 wt% of dead-burnt magnesia (<45 μm, 95 wt% MgO, $CaO/SiO_2 = 0.37$, Magnesita Refratários S.A., Brazil), 7 wt% of reactive alumina (CL370, Almatis, USA) and 18 wt% of fine (<200 μm) tabular alumina (Almatis, USA). For all castables, coarse tabular alumina (<6 mm, Almatis, USA) was used as aggregates. Calcium aluminate cement (Secar71, Kerneos, USA) or hydratable alumina (AlphaBond300, Almatis, USA) were used as binders and silica fume (971U, Elkem, Norway) was added in some compositions.

The main differences among the *in situ* (IS) spinel-forming compositions were the silica fume content (1 wt% – IS-6C1S, or silica fume-free – IS-6C0S, both bonded with 6 wt% of calcium aluminate cement – 6C) and the binder source (6 wt% of calcium aluminate cement – IS-6C1S, or 6 wt% of hydratable alumina – IS-6H1S, both containing 1 wt% of silica fume). For the pre-formed (PF) spinel containing composition, 21 wt% of synthetic spinel was added (<500 μm, Almatis, USA), and it was bonded with 6 wt% of calcium aluminate cement, also adding 1 wt% of silica fume (PF-6C1S). All compositions were dispersed with 0.2 wt% of a polycarboxylate-based additive, in order to ensure suitable shaping under vibration (80% of initial vibration flow). The water content was in the range of 3.9–4.1 wt% for the cement-containing compositions and 5.3 wt% for the hydratable alumina one. Table 1 presents the compositions of these castables.

Table 1
General information of the castables compositions.

Designed compositions	IS-6C1S	IS-6C0S	IS-6H1S	PF-6C1S
Raw materials				
Tabular ($d < 6$ mm) and reactive alumina ($d_{50} = 4$ μm)	87	88	93	72
Dead-burnt MgO ($d < 45$ μm)	6	6	6	–
Calcium aluminate cement	6	6	–	6
Hydratable alumina	–	–	6	–
Silica fume	1	–	1	1
Pre-formed spinel ($d < 1$ mm)	–	–	–	21
Chemical composition				
Al_2O_3	91.2	92.2	93.0	91.2
MgO	6.0	6.0	6.0	6.0
CaO	1.8	1.8	–	1.8
SiO_2	1.0	–	1.0	1.0

Table 2
Chemical composition of the secondary metallurgy slag used in this work.

Oxides	Al_2O_3	MgO	CaO	SiO_2	MnO	Fe_2O_3
Content (wt%)	29.6	3.1	44.9	5.3	2.2	4.9

After mixing, the castables were molded as rectangular bars (150 mm × 25 mm × 25 mm), cured at 50 °C for 24 h (humid environment for cement and room conditions for hydratable alumina) [21], dried at 110 °C for 24 h, calcined at 600 °C for 5 h and, then, fired at 1500 °C for 5 h in order to ensure the *in situ* spinel and calcium hexaluminate (CA_6) formation [22].

After firing, the castables were evaluated in terms of apparent porosity and permanent linear expansion (PLE). The apparent porosity was measured using the Archimedes technique in kerosene, whereas the expansion was evaluated by the difference between the initial and final length of bar samples, before and after firing at 1150, 1300 and 1500 °C for 5 h. In addition, the pore diameter distribution was measured by mercury intrusion porosimetry (Aminco, Model 5-7118, USA).

Concerning the corrosion tests, the fired bars (1500 °C for 5 h) were cut into small cups (25 mm height and both, 10 mm central inner diameter and depth). Afterwards, the samples were filled in (5 g of slag to roughly 40 g of refractory) with a mixture of 90 wt% of a steel ladle basic slag (Table 2) and 10 wt% of iron oxide (95 wt% of purity). Table 2 indicates the composition of slag without adding further FeO_x. The corrosion cup tests (error of 10%) were conducted in a vertical tube furnace with a controlled atmosphere (HTRV 100-250/18 GERO, Germany). The tests were carried out at 1550 °C for 2 h in an oxidizing atmosphere (95 vol% CO_2 and 5 vol% CO). This CO_2/CO ratio was selected instead of air in order to keep the same environmental conditions in all tests and also due to equipment constraints, which did not allow to select 100 vol% of CO_2.

After testing, the samples were cut and polished for scanning electron microscopy (JEOL JSM – 5900 LV, the Netherlands) evaluation. In addition, wear and infiltration parameters were attained (by the analysis of the cross section image of the samples, using the Image J 1.42q software, Wayne Rasband, National Institutes of Health, USA) in order to quantify the corrosion damage, as follows:

Wear index (%): this parameter corresponds to the refractory's mass percentual loss after the interaction of this material with the molten slag. The index is measured considering the distance between the original internal surface of the castable sample (dotted line – Fig. 1a) and the resultant one after the corrosion test (solid line located at the sides of the sample (slag surface) – Fig. 1a), divided by the initial overall side dimension. The measurements were carried out only at the right and left sides of the images (as in some cases the corroded zone at the bottom of the samples were not clearly defined) and an average value of the refractory's wear was attained.

Penetration index (%): it is the relative infiltrated area of the castable. The original and the infiltrated (as pointed out by the highlighted area in Fig. 1b) areas of the sample cross section were measured and, after that, the percentage of the slag penetration was calculated.

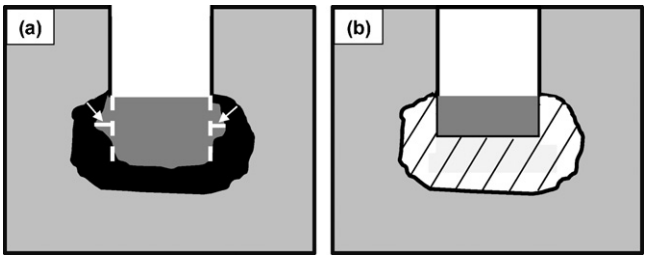

Fig. 1. Selected parameters for (a) wear and (b) penetration area. The arrows in part (a) indicate the corroded depth in the sample.

3. Results and discussion

3.1. Castable characterization

The castable microstructures after thermal treatment at 1500 °C for 5 h are shown in Fig. 2. The IS-6C1S sample showed calcium hexaluminate (CA_6) grains mainly at the edge of tabular alumina grains (but also in the interior of tabular alumina grains and in the matrix) and *in situ* spinel grains throughout the castable matrix. The non-crystalline phase (derived from the liquid formed at a high temperature) was also spread into the castable matrix, as it contained silica fume and calcium aluminate cement in its composition. For the IS-6C1S samples, the CA_6 was partially formed at the border of alumina grains, whereas for the IS-6C0S this phase was fully generated by the reaction with tabular alumina (aggregates). In addition, this castable did not present liquid formation during the thermal treatment and a low amount of CA_2 was detected by spot EDX. The absence of silica fume might have restricted the CA_6 generation only at the edge of tabular alumina grains [15].

Concerning the hydratable alumina-bonded castable (IS-6H1S), it did not show CA_6, as no CaO was added, but *in situ* spinel and most likely an amorphous phase were detected in its matrix by SEM element chemical mapping. Nevertheless, the formed liquid phase was different from the one detected in the IS-6C1S composition, as this castable did not contain CaO. For PS-6C1S, calcium hexaluminate grains were mostly formed in the matrix and the amount of fine spinel (<45 μm) was less in this castable sample than for the other compositions (16.5 wt% instead of ∼21 wt%, in relation to the overall castable wt%). Higher amount of finer pre-formed spinel could not be added, due to the particle size distribution design restrictions.

As the corrosion attack takes place firstly in the castable matrix (<200 μm), Table 3 indicates the chemical composition differences among the four castables. After firing at 1500 °C for 5 h (before the corrosion cup-tests), the available fine alumina present in the castables IS-6C1S and IS-6C0S was mainly consumed for the *in situ* spinel formation, as it precedes the CA_6 generation [22]. For the 6 wt% of MgO containing samples, 15 wt% of Al_2O_3 is required for the stoichiometric spinel formation and, therefore, coarse tabular alumina was also

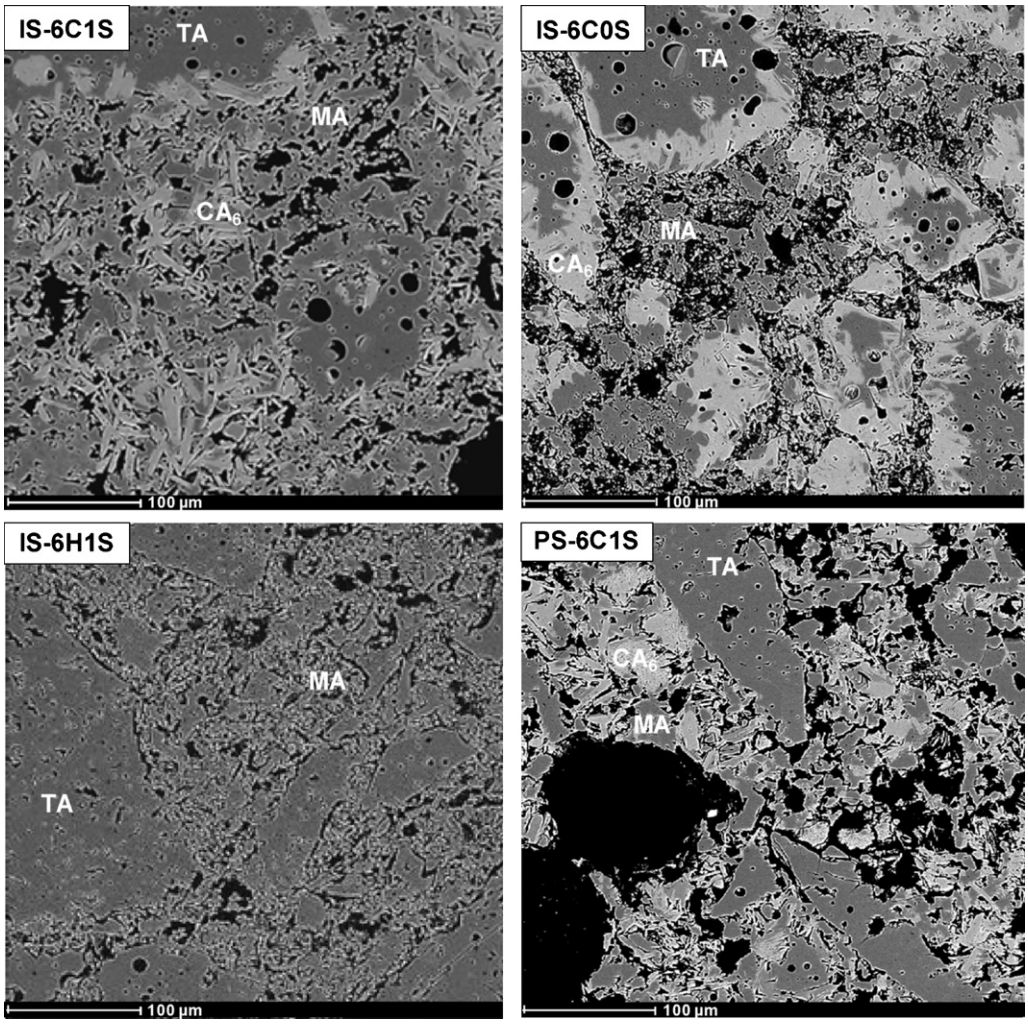

Fig. 2. Castable microstructures after firing at 1500 °C for 5 h (before corrosion cup-tests). TA, tabular alumina; MA, spinel; CA_6, calcium hexaluminate.

consumed for the overall CA_6 generation. Moreover, the spinel of IS-6C1S composition was an alumina-rich type (77 wt% Al_2O_3 – 23 wt% MgO, according to spot EDX analyses results [15]) and, thus, there was a greater likelihood for higher content of free alumina in the matrix in composition IS-6C0S than in the IS-6C1S one.

Considering Table 3 and disregarding the alumina required for the *in situ* spinel formation and even for its alumina enrichment, a high amount of fine alumina would still be present in the IS-6H1S sample, as no CA_6 formation would take place. For the castable PS-6C1S, the fine alumina was added to ensure similar CA_6 formation as for the spinel-forming castables and, therefore, almost no free alumina was available in the sample's matrix after firing at 1500 °C. Table 4 summarizes the location and amount of the main phases for these castables.

Table 3
Differences among the castable matrix (<200 μm) chemical compositions for the four samples.

	Amount of oxides and pre-formed spinel (%)			
	IS – 6C1S	IS – 6C0S	IS – 6H1S	PS – 6C1S
Al_2O_3	77	79	81	34
CaO	5	5	0	6
SiO_2	3	0	3	3
MgO	16	16	17	0
$MgAl_2O_4$	0	0	0	56

Besides the microstructure and phase evaluation, physical properties that could affect the corrosion behavior were also measured. As this class of castable shows expansion during its firing [23–25], permanent linear expansion (PLE) and apparent porosity were analyzed as a function of temperature (Fig. 3). As an initial reference, the apparent porosity level (%) after drying at 110 °C for 1 day was: 5.3 ± 0.7 for IS – 6C1S; 9.5 ± 0.8 for IS – 6C0S; 6.1 ± 0.1 for IS – 6H1S; and 9.0 ± 1.2 for PS – 6C1S. Although these differences, due to firing, all castables showed similar porosity after firing at 1150 °C for 5 h.

For all spinel-forming compositions (IS), the PLE and apparent porosity increased from 1150 to 1300 °C, as this is the temperature range in which spinel formation takes place. After firing at 1500 °C, the castable IS-6C1S showed the highest expansion and apparent porosity values, as a consequence of magnesia and calcium aluminate addition, leading not only to

Table 4
Characteristics of the main castable phases after firing at 1500 °C for 5 h (before the cup-tests).

Composition	Alumina	Spinel ($MgAl_2O_4$)		CA_6		Amorphous phase
	Amount in the matrix	Location	Amount[a]	Location	Amount[a]	Oxide present
IS – 6C1S	+	Matrix	21	Matrix/aggregates (TA)	16	C, M, A, S
IS – 6C0S	++	Matrix	18	Coarse and fine aggregates (TA)	18	–
IS – 6H1S	+++	Matrix	21	–	0	A, M, S
PS – 6C1S	–	Matrix/aggregates[b]	21	Matrix	18	C, A, S

TA, tabular alumina, C, CaO, A, Al_2O_3, M, MgO, S, SiO_2.
[a] XRD quantitative analyses (Rietveld method).
[b] 16.5 wt% < 200 μm (4.5 wt% > 200 μm, leading to 21 wt% of pre-formed spinel in total).

the *in situ* spinel formation, but also to the CA_6 one [22,24,26]. The absence of silica fume reduced the overall PLE and apparent porosity of the IS-6H0S samples at 1500 °C.

Nevertheless, the expansion and porosity was mainly controlled by replacing calcium aluminate cement with hydratable alumina. The absence of cement and the sinterability of this binder source [21] resulted in the lowest PLE and apparent porosity after firing at 1500 °C, including the pre-formed spinel-containing castable (PS-6C1S). Although this sort of spinel addition would increase the castable volumetric stability [5], the calcium aluminate cement presence increased its expansion from 1300 to 1500 °C. Considering these results and the amount of open pores generated after firing at 1500 °C, the hydratable alumina-containing castable would be, by this criterion, the one with the highest slag penetration resistance.

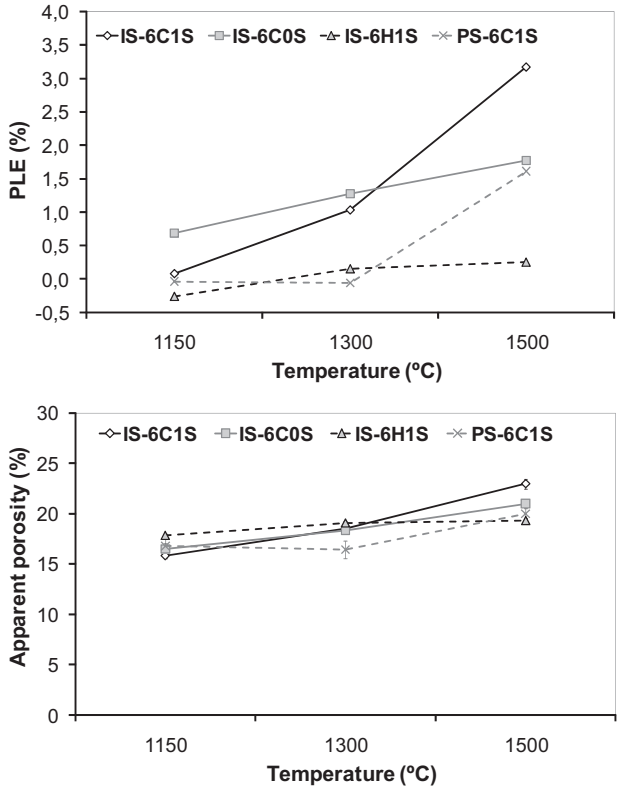

Fig. 3. Permanent linear expansion (PLE) and apparent porosity as a function of the firing temperature (1150, 1300 or 1500 °C) of the four evaluated compositions.

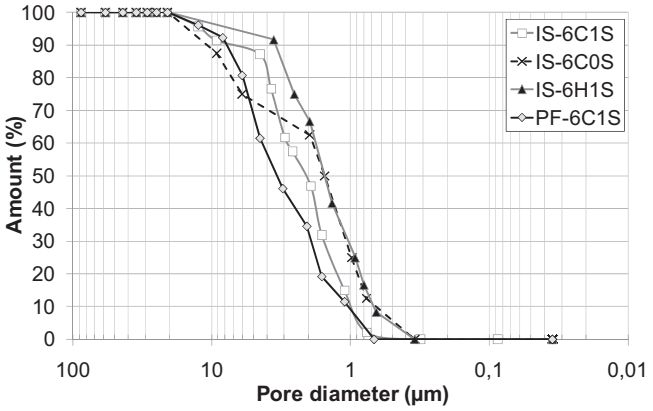

Fig. 4. Pore diameter distribution of the four evaluated compositions.

According to Fig. 2, the pore distribution and sizes for each castable are very different, most likely due to the reactions among the several refractory matrix components, the distinct expansion mechanism and particle packing. In order to quantify this aspect, Hg porosimetry was carried out and the results are shown in Fig. 4. All castables presented pore diameters smaller than 20 μm. The pre-formed spinel castable (PS-6C1S) showed the highest amount of large pores, pointing out a greater likelihood for slag infiltration. Among the *in situ* spinel-containing compositions, the hydratable alumina-bonded one (IS-6H1S) had the highest amount of small pores and, thus, an opposite behavior compared to the PS-6C1S one. The silica fume-free castable (IS-6C0S) also showed a great content of fine pores and the IS-6C1S (containing 1 wt% of silica fume) presented an intermediate profile. Taking this aspect into consideration, the castable IS-6H1S would again be more resistant to slag penetration.

3.2. Slag corrosion behavior: wear and infiltration indexes

Fig. 5 presents the castable corrosion profiles after the cup-tests [27], whereas the penetration and corrosion indexes are indicated in Fig. 6. Remaining slag was detected in the inner part of the IS samples, indicating that it did not fully infiltrate and/or react with the castables. On the other hand, for the pre-formed spinel-containing composition, a complete slag infiltration took place and, due to the reactions between the liquid and the refractory, the sample lost its original shape and

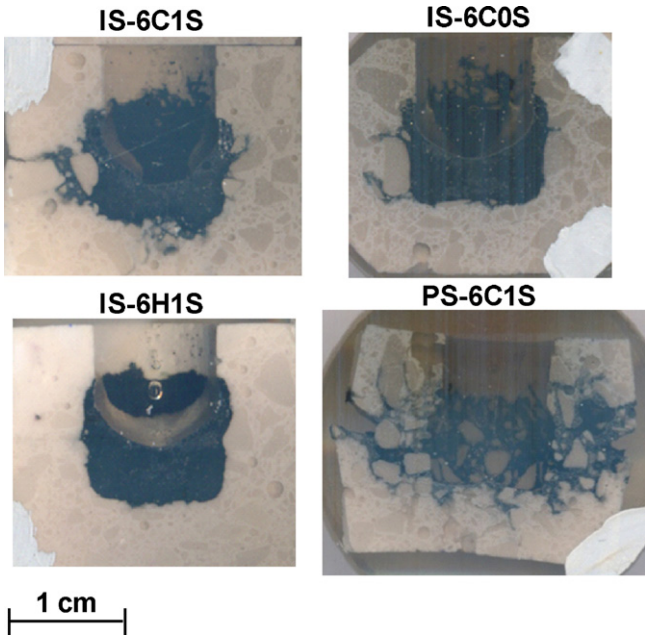

Fig. 5. Castable corrosion profiles after the cup-tests [27].

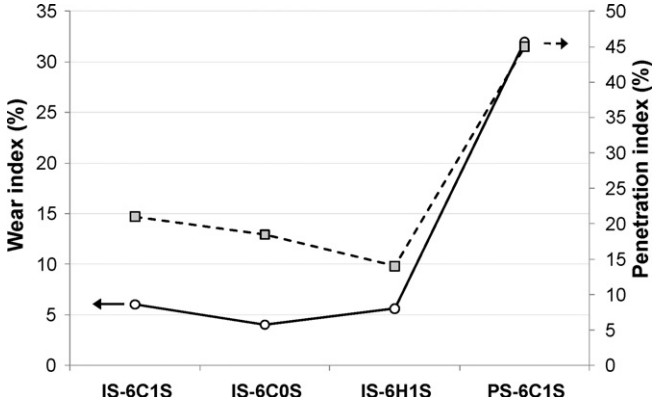

Fig. 6. Wear and slag penetration indexes of the four corroded castables.

dimensions due to a high macrocracking effect. Moreover, tabular alumina aggregates are clearly observed in PS-6C1S, indicating an intense wear of this castable matrix composition.

Conversely, the IS-6C0S and IS-6H1S castables kept their original cross section, without presenting macrocracks. Concerning the penetration and wear indexes, both samples showed low corrosion, but the hydratable alumina-bonded composition (IS-6H1S) showed the lowest liquid penetration. This result is in tune with the physical parameters analyzed before, as the IS-6H1S composition showed lower expansion and apparent porosity values after firing at 1500 °C, as well as a high content of small pores (more than 90 vol% was lower than 4 μm – Fig. 4). Additionally, the pore diameters of the IS-6C0S samples were also small (roughly 60 vol% lower than 2 μm – Fig. 4). Therefore, not only chemical aspects (i.e., the absence of silica fume or the amount of fine alumina available in the castables matrix, as will be discussed later), but also physical properties, played their roles to inhibit the slag penetration, acting as a physical barrier for further corrosion.

For the IS-6C1S composition, an intermediate behavior took place: a partial loss of its original cross section and macrocracks were detected (but to a lower extent than the PS-6C1S castable), whereas its wear index was just slightly higher than the ones for the IS-6C0S or IS-6H1S compositions. According to these results, these later castables showed the best corrosion resistance among the four different evaluated compositions.

Another aspect that matches their best corrosion resistance is the evaluation by SEM of the remnant slag after the cup-tests. Fig. 7 shows micrographs of the remnant slag after cooling and the phases detected by spot EDX analyses; results from the latter are presented in Table 5. The remaining slag of the castables IS-6H1S and IS-6C0S showed similar phases to the ones predicted by the thermodynamic analyses after liquid–solid contact [27], indicating that lower reaction between the slag and the refractories took place. On the other hand, for castables IS-6C1S and PS-6C1S, the remained slag was chemically different than the predicted ones [27] and, therefore higher interaction between the slag and the refractories was likely before attaining the oxide saturation equilibrium.

3.3. Slag–refractory chemical interaction

The SEM images of the corroded region for the four castables are shown in Fig. 8. In general, the final microstructure after the cup-tests were different for each composition, but some similar features can be highlighted. Except for the IS-6H1S castable, continuous and well defined calcium aluminate layers were detected at the edge of tabular alumina grains (dotted lines in the figures), pointing out an indirect corrosion mechanism, as previous reported by the literature [10,18,28,29]. For all samples, the main crystalline phases (spinel and also calcium aluminates) presented iron and manganese in their solid solution. This slag oxide entrapment is one of the main purposes of adding spinel to refractory castables which are being used in contact with basic slag.

For castable IS-6C1S, the phase sequence $CA_6/CA_2/CA$ was detected at the border of the alumina aggregates. The CA_6 grains showed platelet morphology, comprised as layers of roughly 100 μm. Pores were detected at the interface between the CA_6 and the CA_2 layers, which mainly presented an angular shape. On the other hand, the pores of the CA_6 layer close to the tabular alumina showed a similar rounded aspect compared to the ones contained in these aggregates. The CA_2 layer was intensively compact and finer than the CA_6 one. Furthermore, CA_2 was not only detected in this layer, but also at the slag interface. At the slag–refractory interface, spinel was detected with a cubic morphology and particle size close to 25 μm. In the area closer to the slag, FeO_x and MnO concentration were higher than in deeper refractory regions and CA was observed, but its morphology could not be clearly defined. The amount of alumina was reduced from the slag–refractory interface up to the slag region, pointing out that the refractory aggregates were the alumina source for the calcium aluminate generation.

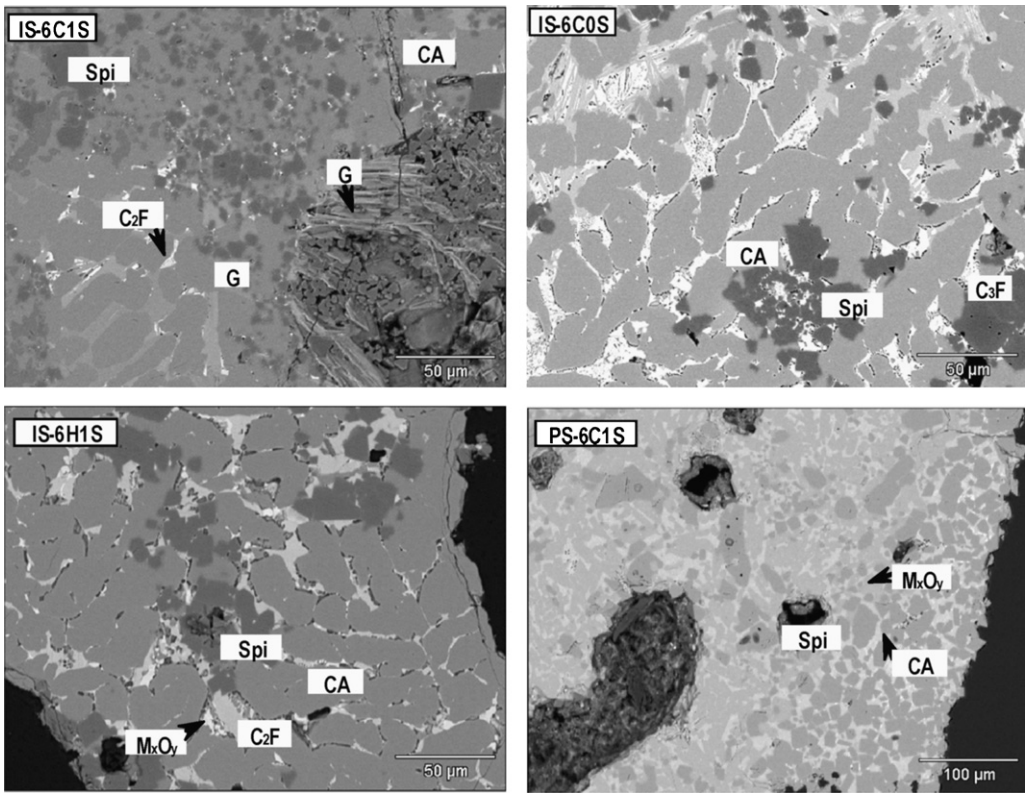

Fig. 7. Remaining slag at the interface of the refractory after the corrosion cup-tests for the four castables. G, gehlenite (C_2AS); Spi, spinel (MA); M_xO_y, MgO + MnO + Fe_2O_3 (IS-6H1S) and MgO + Al_2O_3 + Fe_2O_3 + CaO (PS-6C1S).

The same layered structure was detected in the castable IS-6C0S, with similar phase distribution to the one mentioned above. Nevertheless, one of the differences was the CA_6 layer at the edge of tabular alumina grain, which, in this composition, was compact and had a low porosity level (but again, similar to those rounded inside the tabular alumina aggregates). The thickness of this layer was smaller (~25 μm) than the one detected for IS-6C1S (~100 μm) and the CA_6 grains showed platelet shapes. The CA_2 layer was also strongly compact and, due to this reason, its morphology could not be defined. After this, a CA layer was formed (with a thickness slightly higher than 10 μm). Spinel was detected in this region of the sample (between CA layer and the slag zone) presenting high iron and manganese concentration in its composition.

For the IS-6H1S, this calcium aluminate layered structure was not clearly detected. However, the phases observed close to tabular alumina grains were similar to the ones previously mentioned: CA_6 platelets, CA_2, spinel, but also a phase or melt containing CaO, Al_2O_3 and SiO_2 that could be gehlenite, according to the EDX analysis.

Table 5
Slag composition by SEM/EDX analysis after the corrosion tests [27].

	IS-6C1S	IS-6C0S	IS-6H1S	PS-6C1S
CA	✓	✓	✓	✓
CA_2	✓			✓
Ghelenite (CA_2S)	✓			
Ghelenite or glassy phase		✓	✓	✓
C_2A_4S	✓			
Glassy phase	✓			
C_xA_y[a] with Fe_2O_3 or CA with Fe_2O_3 ss		✓	✓	
C_3A c/Fe_2O_3		✓		
C_2F c/A_2O_3 ss			✓	
Spinel	✓	✓	✓	✓
Fe_2O_3	✓			
Oxides mixture[b]		✓	✓	✓

[a] C_xA_y could be: $C_{12}A_7$, C_2A or C_3A.
[b] IS-6C0S and IS-6H1S: MgO + MnO + Fe_2O_3; PS-6C1S: MgO + Al_2O_3 + Fe_2O_3 + CaO.

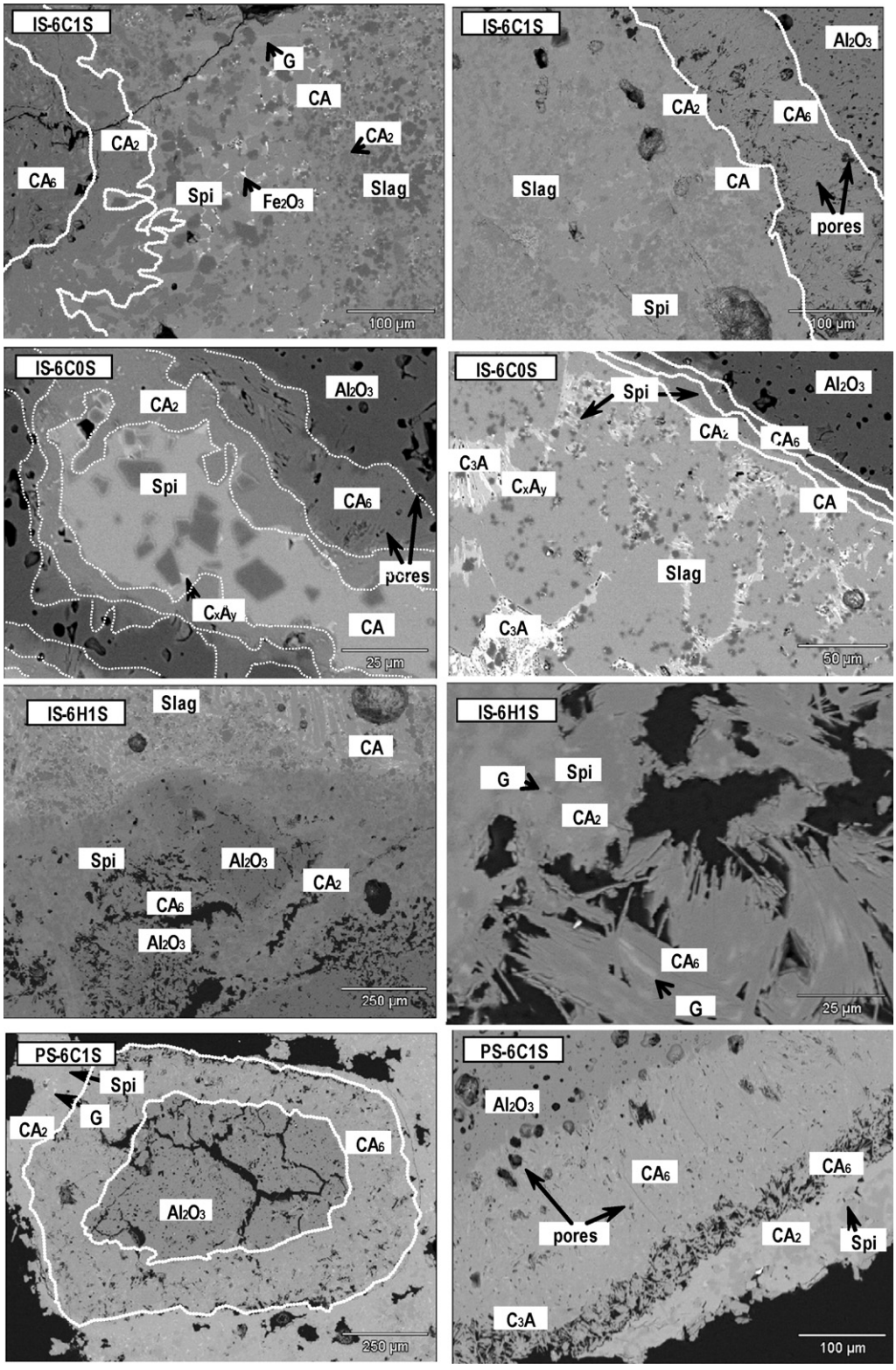

Fig. 8. Corroded region of the four compositions. G, gehlenite (C_2AS); Spi, spinel (MA); C_xA_y, $C_{12}A_7$, C_2A or C_3A.

For the pre-formed spinel-containing composition (PS-6C1S), the highest CA_6 layer thickness was observed (~250 μm) at the edge of alumina aggregates, among all evaluated castables. Besides this, the CA_6 features (morphology and porosity) were similar to the ones of IS-6C1S castable. CA_2 was detected after the CA_6 layer, however a clearly layered region such as the previous compositions (IS-6C1S and IS-6C0S) was not observed. CA was not found in this castable close to the tabular alumina grains, whereas spinel was detected, but its morphology was not easily defined, due to its brighter aspect, as a consequence of the presence of iron oxide in solid solution.

3.4. Slag corrosion mechanism for the testing conditions and selected compositions

Considering the experimental features of the four corroded samples and previous thermodynamic calculations [27], a corrosion mechanism for the produced castables can be stated, considering physical, mechanical and chemical aspects. Based on the attained results, the corrosion of these castables takes place through the formation of layers of the slag–refractory reaction products. The following events are proposed:

- The slag infiltrates into the refractory castables through the available ways (pores, cracks, grain boundaries, etc.) and the effectiveness of this infiltration depends on the castable physical properties, such as apparent porosity and pore diameters. According to Figs. 3 and 4, the IS-6C1S would be more prone to infiltration considering its higher porosity after firing at 1500 °C, whereas the PS-6C1S composition would show high infiltration due to the large pore higher content. Matsushita et al. [30] stated that this later parameter would determine the liquid penetration. Therefore, the pre-formed spinel-containing castable would show higher slag physical infiltration. Conversely, castables IS-6H1S and IS-6C0S (mainly the first one) showed a lower penetration trend;
- The castable matrix (which comprises fine grains) is partially or fully dissolved [27] increasing the content of alumina, calcia, magnesia and silica in the liquid slag, changing its composition and viscosity. This physical process is determined by the matrix composition and microstructure, as summarized in Table 4. For the IS-6H1S composition, the slag is not enriched with calcia, whereas for the IS-6C0S, its silica content is kept constant, according to Table 3. The fine alumina content also changes among the four compositions, as its availability depends on the *in situ* spinel and CA_6 formation. The PS-6C1S samples, which comprise a lower amount of fine spinel than the others, would lead to lower MgO enrichment in the slag. Moreover, the presence of silica fume (and thus liquid phase), also induces further corrosion, which should be detected for the IS-6C1S, IS-6H1S and PS-6C1S. Nevertheless, previous work by the authors [27] pointed out that the liquid viscosity of composition IS-6H1S would be higher and, as a consequence, this castable would present higher corrosion resistance;
- If the slag–matrix mix is not saturated with alumina, then the castable aggregates are subject to surface dissolution, leading to the reaction between slag components and alumina and to the calcium aluminate phase generation. The IS-6H1S composition is the one that contains the higher amount of fine alumina and, therefore, its aggregates are less attacked by the slag [27]. This statement is supported by the absence of calcium aluminate layers at the border of tabular alumina grains in this composition;
- The first stable solid phase formed in this system is CA_2, according to thermodynamic predictions [27]. This phase was detected by SEM as a dense layer at the border of tabular alumina aggregates, but also dispersed in regions close to the slag. The highest the CA_6 and CA_2 contents available in the castable matrix after firing, the largest was the CA_2 thickness. Furthermore, higher slag infiltration (due to physical parameters) would also lead to greater calcia and alumina contents. Therefore, a higher amount of CaO would be available in the pre-formed spinel-containing castable (PS-6C1S). In principle, neither IS-6C0S nor IS-6H1S could lead to this calcia enrichment, as both did not comprise CaO in their castable matrix.
- Due to the thermodynamic incompatibility of CA_2 and Al_2O_3 phases (i.e., tabular alumina aggregates) when in contact, they react leading to CA_6 formation. During the progress of the CA_2–Al_2O_3 reaction, the CA_6 stability increases regarding the CA_2 one [27] and its layer thickness increases by two routes:
  (i) CA_6/CA_2: the reaction proceeds via liquid state. Similarly to the CA_2, the CA_6 layer would be thicker for higher calcia availability (from the slag and also from the original castable matrix). Therefore, the pre-formed spinel castable (PS-6C1S) showed the higher CA_6 layer thickness, followed by IS-6C1S, IS-6C0S and, then, IS-6H1S (absence of this layer).
  (ii) CA_6/aggregate: the reaction takes place by solid state, as there is no contact with liquid (since the previous CA_6 layer formed act as a physical barrier for further reaction). This aspect is in agreement with the pore morphology in the CA_6 layer close to the aggregates, which kept the original shape of tabular alumina pores (Fig. 8),
- The formation of the CA_2 and CA_6 layers inhibited further corrosion and, according to the literature [18,28], the thicker and more continuous these layers are, the more efficient the aggregate protection is. Nevertheless, as the CA_2 and CA_6 formations are followed by volumetric expansion [10,15] and their intense generation could lead to cracks, further infiltration would take place. Therefore, despite the castable physical properties (porosity and pore sizes), a higher amount of formed CA_6 and CA_2 might ease the slag penetration and lower the castable integrity. This mechanical effect can be

Table 6
Physical and chemical characteristics of the castables, correlated with the attained corrosion results.

Composition	Physical properties	Chemical features			Corrosion results	
	Apparent porosity/pore diameters	Al_2O_3 content (matrix)	CA_6 content (matrix)	Liquid phase	Wear	Penetration
IS – 6C1S	Highest/intermediate	Low	High	Yes	Low	Intermediate
IS – 6C0S	Low/low	High	Low	No	Low	Low
IS – 6H1S	Lowest/lowest	Highest	Absent	Yes	Low	Lowest
PS – 6C1S	Low/high	Absent	Highest	Yes	High	Highest

critical to the castable corrosion performance, overcoming physical or chemical aspects, as observed for the pre-formed spinel-containing composition (PS-6C1S). This expansive behavior and the crack formation were less critical for the IS-6C1S composition, but some macrocracks were detected, indicating that the CA_6 layer thickness was slightly above an optimal value, that would ensure the aggregate protection. On the other hand, the silica fume free castable (IS-6C0S) showed tiny CA_6 and CA_2 layers, without signs of negative effects related to this phase generation.

- In parallel to the calcium aluminate phase formation, the spinel grains in the castable matrixes were fully dissolved and recrystallized when in contact with liquid slag [27] and entrapped slag ions such as Fe and Mn, increasing the local content of silica in the slag and, then its viscosity, which inhibits further penetration [1–4]. Nevertheless, no continuous layer of spinel (that could act as a physical barrier) was detected due to the low magnesia content [29].

As the amount of fine spinel in the pre-formed spinel-containing castable (PS-6C1S) was lower than in the others and as this castable comprised silica fume in its composition [14], further experiments are still required to clearly identify the effect of the spinel incorporation route. Moreover, the calcium aluminate layer formations seem to be the most relevant corrosion aspect for this sort of castable and, thus attention should be drawn when designing the castable chemical composition and particle size distribution.

3.5. Castable raw material design

Table 6 summarizes the main physical and chemical effects that affected the corrosion resistance of the evaluated composition. According to this table, low penetration results were attained for the samples that showed low apparent porosity, but mainly smaller pore diameters. Chemically, the presence of alumina in the matrix, the lack of calcium aluminates and the absence of liquid phase (or formation of liquid phase of high viscosity, for the IS-6H1S) ensured higher corrosion resistance and avoided the generation of thick CA_6 and CA_2 layers, inhibiting expansion and further penetration. This result was attained by generating *in situ* spinel that reduced the pore diameters (although in the cement compositions it led to higher expansion, due to the formation of CA_6 coupled with the spinel generation), by using hydratable alumina as a binder and by the absence of silica fume.

4. Conclusions

The attained results for different spinel-containing castable compositions led to a proposed corrosion mechanism, in which the key-factors that played a role in the basic slag corrosion behavior could be identified. The physical property measurements indicated that the pore diameter distribution is a key aspect to the penetration resistance and better results were attained by using hydratable alumina as a binder, in the absence of silica fume and when *in situ* spinel formation is induced. Furthermore, chemical and microstructural aspects (calcium aluminate phase distribution and the content of calcia and alumina in the castable matrix) also imparted a relevant role to the corrosion behavior and affected the castable mechanical integrity, leading, in two compositions (PS-6C1S and IS-6C1S), to crack generation that would increase the slag infiltration driving force. Therefore, the proper design of the castable composition and the selection of the most suitable raw materials are crucial to ensure a high basic slag corrosion performance.

Acknowledgments

The authors are grateful to the Federation for International Refractory Research and Education (FIRE), Magnesita Refratários S.A. (Brazil) and the Brazilian Research Funding Agency FAPESP. Additionally, the authors are thankful to the Corus Ceramic Research Centre (CRC) for the microstructure evaluation and corrosion test support and to G. G. Morbioli for the castable processing.

References

[1] A. Nagasoe, S.I. Tsurumoto, A. Kitamura, Refractory characteristics of spinels with various MgO contents, Taikabutsu Overseas 11 (3) (1991) 20–28.
[2] J. Mori, M. Yoshimura, Y. Oguchi, T. Kawakami, I. Ohishi, Effect of slag composition on wear of alumina-spinel castable for steel ladle, Taikabutsu Overseas 12 (1) (1992) 40–45.
[3] K. Fujii, I. Furusato, I. Takita, Composition of spinel clinker for teeming ladle casting materials, Taikabutsu Overseas 12 (1) (1992) 4–9.
[4] B. Naigai, O. Matsumoto, T. Isobe, Y. Nishiumi, Wear mechanism of castable for steel ladle by slag, Taikabutsu Overseas 12 (1) (1992) 15–20.
[5] S. Zhang, W.E. Lee, Spinel-containing refractories, in: C.A. Schacht (Ed.), Refractories Handbook, CRC Press, 2004, pp. 215–258.
[6] S. Itose, M. Nakashima, T. Isobe, I. Shimizu, Improvement in the durability of alumina-spinel steel ladle castable containing spinel fine powder, Taikabutsu Overseas 22 (1) (2002) 26–30.
[7] M. Kobayashi, K. Kataoka, Y. Sakamoto, I. Kifune, Use of alumina–magnesia castables in steel ladle sidewalls, Taikabutsu Overseas 17 (3) (1997) 39–44.
[8] T. Yamamura, Y. Kubota, T. Kaneshige, M. Nanba, Effect of spinel clinker composition on properties of alumina-spinel castable, Taikabutsu Overseas 13 (2) (1993) 39–45.
[9] C. Parr, L. Bin, B. Valdelievre, C. Wöhrmeyer, B. Touzo, The advantages of calcium aluminate cement containing castables for steel ladle applications, in: Proceedings of ALAFAR 04, Antígua, Guatemala, CD-ROM, 2004.
[10] J.P. Guha, Reaction chemistry in dissolution of polycrystalline alumina in lime–alumina–silica slag, British Ceramic Transactions 96 (6) (1997) 231–236.
[11] N. Zhou, S. Hu, S. Zhang, Advances in modern refractory castables, China's Refractories 13 (2) (2004) 3–12.
[12] Y.C. Ko, Properties and production of Al_2O_3–spinel and Al_2O_3–MgO castables for steel ladles, Ceramic News 6 (1) (2002) 51–56.
[13] S. Yilmaz, Corrosion of high alumina spinel castables by steel ladle slag, Ironmaking and Steelmaking 33 (2) (2006) 151–156.
[14] M. Schnabel, A. Buhr, R. Exenberger, C. Rampitsch, Spinel: in-situ versus preformed—clearing the myth, Refractories World Forum 2 (2) (2010) 87–93.
[15] M.A.L. Braulio, L.R.M. Bittencourt, J. Poirier, V.C. Pandolfelli, Microsilica effects on cement bonded alumina–magnesia refractory castables,

Journal of the Technical Association of Refractories: Japan 28 (3) (2008) 180–184.
[16] M.A.L. Braulio, P.O. Brant, L.R.M. Bittencourt, V.C. Pandolfelli, Microsilica or MgO grain size: Which one mostly affects the in situ spinel refractory castable expansion? Ceramics International 35 (2009) 3327–3334.
[17] H. Sarpoolaky, S. Zhang, W.E. Lee, Corrosion of high alumina and near stoichiometric spinels in iron-containing silicate slags, Journal of the European Ceramic Society 23 (2003) 293–300.
[18] S. Zhang, H.R. Rezaie, H. Sarpoolaky, W.E. Lee, Alumina dissolution into silicate slag, Journal of the American Ceramic Society 83 (4) (2000) 897–903.
[19] B.A. Vázquez, P. Pena, A.H. de Aza, M.A. Sainz, A. Caballero, Corrosion mechanism of polycrystalline corundum and calcium hexaluminate by calcium silicate slags, Journal of the European Ceramic Society 29 (2009) 1347–1360.
[20] J.E. Funk, D.R. Dinger, Particle packing, part III: discrete versus continuous particle sizes, Interceram 41 (5) (1992) 332–333.
[21] M.A.L Braulio, L.R.M. Bittencourt, V.C. Pandolfelli, Selection of binders for in situ spinel refractory castables, Journal of the European Ceramic Society 29 (13) (2009) 2727–2735.
[22] M.A.L. Braulio, D.H. Milanez, E.Y. Sako, L.R.M. Bittencourt, V.C. Pandolfelli, Expansion behavior of cement bonded alumina–magnesia refractory castables, American Ceramic Society Bulletin 86 (12) (2007) 9201–9206.
[23] Y.C. Ko, J.T. Lay, Thermal expansion characteristics of alumina–magnesia and alumina–spinel castables in the temperature range 800–1650 °C, Journal of the American Ceramic Society 83 (11) (2000) 2872–2874.
[24] K. Ide, T. Suzuki, K. Asano, T. Nishi, Expansion behavior of alumina–magnesia castables, Journal of the Technical Association of Refractories: Japan 25 (3) (2005) 202–208.
[25] M.A.L. Braulio, L.R.M. Bitttencourt, V.C. Pandolfelli, Engineered expansion routes for alumina–magnesia castables, Ceramic Forum International 85 (2008) E77–E82.
[26] M. Fuhrer, A. Hey, W.E. Lee, Microstructural evolution in self-forming spinel/calcium aluminate castable refractories, Journal of the European Ceramic Society 18 (1998) 813–820.
[27] A.P. Luz, A.G. Tomba Martinez, M.A.L. Braulio, V.C. Pandolfelli, Thermodynamic evaluation of spinel containing refractory castables corrosion by a secondary metallurgy slag, Ceramics International (2011) doi:10.1016/j.ceramint.2010.11.043, in press.
[28] H. Sarpoolaky, S. Zhang, B.B. Argent, W.E. Lee, Influence of grain phase on slag corrosion of low-cement castable refractories, Journal of the American Ceramic Society 84 (2) (2001) 426–434.
[29] W.R. Lee, S. Zhang, Melt corrosion of oxides and oxide-carbon refractories, International Materials Reviews 44 (3) (1999) 77–104.
[30] T. Matsushita, T. Ohuchi, K. Mukai, I. Sasaka, J. Yoshitomi, Direct observation of molten steel penetration into porous refractory, Journal of the Technical Association of Refractories: Japan 23 (1) (2003) 15–19.